UNIVERSITÄT SIEGEN

Naturwissenschaftlich Technische Fakultät

University of Siegen

MANUAL
Master Lab Course

Optically detected magnetic resonance (ODMR)

Authors
Philipp Reuschel
Assegid M. Flatae
Florian Sledz
Mario Agio

Department of Physics
Laboratory of Nano-Optics

Contents

List of Figures

List of Tables

Acknowledgements

We would like to thank Navid Soltani and Jan Krause for technical support during the mechanical construction of the setup. We are very grateful for the support provided by the electronical workshop, especially Jens Winter, in designing the microwave circuit and the fabrication of the planar antenna. We would like to thank Professor Christof Wunderlich and Michael Johanning for providing the equipment used to calibrate the microwave circuit. Lastly, we would like to thank Arka Gosh for assistance during the test of the optical setup and his simulation of the microwave antenna.

1 Abstract

In this document, we present a technique called optically detected magnetic resonance (ODMR) by which the electron spin state of a crystal defect in diamond is optically pumped for spin initialisation and readout. We will utilize the nitrogen-vacancy (NV) color center in diamond, to measure the modulus and orientation of an external magnetic field using a confocal microscopy setup. ODMR of NV has applications in magnetometry, sensing, biomedical imaging, quantum information and for the fundamental study of physics.
In the theoretical background, we will introduce the interaction between a two-level system and an external magnetic field. Firstly, we will revise the Zeeman effect, which lays the foundation for magnetic field sensing with the splitting of spectral lines. Secondly, we will discuss one of the key concepts of quantum optics, namely the Rabi model, which describes the effect of an oscillating external magnetic field on a two-level system.
The nitrogen-vacancy center is the physical system used in this experiment. Its creation, optical properties and the working principle of ODMR for measuring external magnetic fields is explained.
The experimental setup, a confocal system combined with a microwave source, is shown and students will have a hands-on experience during this experiment. The basic idea for this student's experiment, particularly the design of the microwave circuit, is taken from [14].
Lastly, students will have to perform data analysis with a program of their choice (e.g., Matlab, Python). This includes plotting and function fitting. A guide through these steps is provided at the end of the manual.

2 Theoretical background

2.1 Zeeman effect

The Zeeman effect (named after Pieter Zeeman) describes the interaction between a spin J (such as an electron) and an external static magnetic field $\boldsymbol{B}$. It can be observed by the splitting of spectral lines into multiple components when an external magnetic field is applied to the physical system. Since the energy split is a function of the field strength, the Zeeman effect can be used to measure magnetic fields.

Classically, one can calculate the magnetic moment $\boldsymbol{p}_m$ of an electron by

$$\boldsymbol{p}_m = -\frac{e}{2m_e} \cdot \boldsymbol{l} \ , \tag{1}$$

where m_e is the electron's mass and $\boldsymbol{l}$ its angular momentum. When such a magnetic moment is brought into an external magnetic field $\boldsymbol{B}$, its potential energy E_{pot} is given by

$$E_{\text{pot}} = -\boldsymbol{p}_m \cdot \boldsymbol{B} \ . \tag{2}$$

When the external magnetic field $\boldsymbol{B}$ is aligned along the z-axis, one finds that

$$E_{\text{pot}} = \frac{e\hbar}{2m_e} m_z B_z \ , \tag{3}$$

since $l_z = m\hbar$. The angular momentum $\boldsymbol{l}$ classically precesses around the z-axis since the torque $\boldsymbol{D} = -(e/2m_e)\,\boldsymbol{l} \times \boldsymbol{B}$ is applied [4].

A similar result can be obtained using quantum mechanics. The Hamiltonian $\hat{\mathrm{H}}$ is defined by

$$\hat{\mathrm{H}} = \gamma \hat{\boldsymbol{J}} \cdot \boldsymbol{B} \ , \tag{4}$$

where γ is the gyro-magnetic moment and $\gamma/2\pi \approx 28.025\,\mathrm{MHz\,mT^{-1}}$. $\hat{\boldsymbol{J}} = \hat{\mathrm{J}}_x \boldsymbol{e}_x + \hat{\mathrm{J}}_y \boldsymbol{e}_y + \hat{\mathrm{J}}_z \boldsymbol{e}_z$ is the total electronic angular momentum operator. For simplicity, we again assume that the external magnetic field is aligned along the z-axis. This leads to

$$\hat{\mathrm{H}} = \gamma B_z \hat{\mathrm{J}}_z \ . \tag{5}$$

To find the energy shift ΔE caused by the coupling between static external magnetic field and a spin, we need to find eigenvalues for the equation

$$\hat{\mathrm{H}} \left| j, m_j \right\rangle = E \left| j, m_j \right\rangle \ , \tag{6}$$

where j is the angular momentum number of the particle and m_j its magnetic spin number. We can solve this problem for the case of spin-1/2- and spin-1-particles using matrix representation, defined by

$$\hat{\mathrm{J}}_z = \frac{\hbar}{2}\begin{pmatrix}1 & 0\\ 0 & -1\end{pmatrix} \quad \text{and} \quad \hat{\mathrm{J}}_z = \hbar\begin{pmatrix}1 & 0 & 0\\ 0 & 0 & 0\\ 0 & 0 & -1\end{pmatrix} , \tag{7}$$

respectively. For spin-1/2 we find $m_j = \pm 1/2$ and for spin-1 we find $m_j \in \{-1, 0, 1\}$ with

$$\hat{\mathrm{J}}_z \left|j, m_j\right\rangle = \hbar m_j \left|j, m_j\right\rangle . \tag{8}$$

Therefore, the energy splitting ΔE of the Zeeman effect can be calculated simply by

$$\Delta E = \Delta m_j \, \hbar\gamma B_z. \tag{9}$$

2.2 Rabi model

The Rabi model (named after Isidor Isaac Rabi) describes the interaction between a two-level quantum system and a classical oscillating magnetic field. It is very famous since it delivers an intuitive way of dealing with a two-level system. In this chapter, we will briefly go over the basic idea of the model and coarsely do some derivation which leads us to the results. A more detailed (and alternative) calculation can be found in [7] or on quantum optics text books.

2.2.1 Co-rotating frame and time evolution

To start, we take a static external magnetic $B_\parallel$ aligned along the z-axis so we can (according to the Zeeman model) define the ground state as $|0\rangle \coloneqq |-z\rangle$ and excited state as $|1\rangle \coloneqq |+z\rangle$. Without an oscillating field, we can write

$$\hat{\mathrm{H}}_\parallel = \gamma B_\parallel \hat{\mathrm{J}}_z = \frac{\hbar\omega_0}{2}(|e\rangle\langle e| - |g\rangle\langle g|) = \frac{\hbar\omega_0}{2}\sigma_z , \tag{10}$$

where $\omega_0 = \gamma B_\parallel$. Now we can add the oscillating field $\boldsymbol{B}(t) = \boldsymbol{B}_\perp \cos(\omega t)$, which lies within the xy-plane with an azimutal angle ϕ.

$$\begin{aligned}
\hat{\mathrm{H}}_\mathrm{S} &= \frac{\hbar\omega_0}{2}\sigma_z - \gamma B_\perp \frac{\hbar}{2}\cos(\omega t)[\cos(\phi)\sigma_x + \sin(\phi)\sigma_y] && (11)\\
&= \frac{\hbar\omega_0}{2}\sigma_z - \frac{\hbar\Omega}{2}\cos(\omega t)[\cos(\phi)\sigma_x + \sin(\phi)\sigma_y] && (12)\\
&= \frac{\hbar\omega_0}{2}\sigma_z - \frac{\hbar\Omega}{2}[\exp(-i(\omega t+\phi))\sigma_+ + \exp(+i(\omega t+\phi))\sigma_-] , && (13)
\end{aligned}$$

where $\Omega = \gamma B_\perp$ is the Rabi frequency.

We now use the interaction picture to transform this Hamiltonian into a co-rotating frame which oscillates at the same frequency ω as the varying magnetic field $B_\perp$. To do this, we define

$$\hat{\mathrm{H}}_0 = \hat{\mathrm{H}}_\parallel = \frac{\hbar\omega_0}{2}\sigma_z \tag{14}$$

$$\hat{\mathrm{H}}_{\mathrm{int}} = -\frac{\hbar\Omega}{2}[\exp(-i(\omega t+\phi))\sigma_+ + \exp(+i(\omega t+\phi))\sigma_-] \tag{15}$$

and use the unitary

$$\hat{\mathrm{U}}_{\mathrm{RF}} = \exp(-i\frac{\omega}{2}t\,\sigma_z) \tag{16}$$

to transform the states $|\Psi\rangle$ from the Schrödinger (S) picture into the rotating frame (RF), such that

$$|\Psi_{\mathrm{RF}}(t)\rangle = \hat{\mathrm{U}}_{\mathrm{RF}}^\dagger\,|\Psi_{\mathrm{S}}(t)\rangle\ . \tag{17}$$

After some calculation, we arrive at the Hamiltonian in the rotating frame

$$\hat{\mathrm{H}}_{\mathrm{RF}} = -\frac{\hbar\Delta}{2}\sigma_z + \frac{\hbar\Omega}{2}[\exp(-i\phi)\sigma_+ + \exp(i\phi)\sigma_-] \tag{18}$$

$$= -\frac{\hbar\Delta}{2}\sigma_z + \frac{\hbar\Omega}{2}[\cos(\phi)\sigma_x + \sin(\phi)\sigma_y]\ , \tag{19}$$

with the detuning $\Delta = \omega - \omega_0$ and the Rabi frequency Ω.

One finds the time evolution of an initial state $|\Psi_{\mathrm{RF}}(0)\rangle$

$$|\Psi_{\mathrm{RF}}(t)\rangle = \hat{\mathrm{U}}_{\mathrm{Rabi}}(t)\,|\Psi_{\mathrm{RF}}(0)\rangle = \exp\left(-\frac{i}{\hbar}\hat{\mathrm{H}}_{\mathrm{RF}}t\right)|\Psi_{\mathrm{RF}}(0)\rangle \tag{20}$$

is simply a rotation on the Bloch sphere with

$$\hat{\mathrm{U}}_{\mathrm{Rabi}}(t) = \exp\left(-i\frac{\boldsymbol{\Omega}_{\mathrm{tot}}}{2}\cdot\boldsymbol{\sigma}t\right) \tag{21}$$

$$= \cos\left(\frac{\Omega_{\mathrm{tot}}}{2}t\right)\mathbb{1} - i\frac{\Omega}{\Omega_{\mathrm{tot}}}\sin\left(\frac{\Omega_{\mathrm{tot}}}{2}t\right)[\cos(\phi)\sigma_x + \sin(\phi)\sigma_y]\ , \tag{22}$$

where $\boldsymbol{\Omega}_{\mathrm{tot}} = -\Delta\boldsymbol{e}_z + \Omega\boldsymbol{e}_\perp$ and $\Omega_{\mathrm{tot}} = \sqrt{\Delta^2+\Omega^2}$ is the generalized Rabi frequency.

2.2.2 Rabi oscillations

We will now consider a two-level system which is initially in the ground state $|-z\rangle$ and is driven by an external oscillating magnetic field B_x, which is aligned along the x-axis. We are interested in the probability P_e to find the system in the excited state $|+z\rangle$ after time T has passed:

$$P_{\mathrm{e}}(T) = |\langle +z|\, \hat{\mathrm{U}}_{\mathrm{Rabi}}\, |-z\rangle\, |^2 \tag{23}$$

$$= \left| \langle +z| \left[\cos\left(\frac{\Omega_{\mathrm{tot}}}{2} T\right) \mathbb{1} - i \frac{\Omega}{\Omega_{\mathrm{tot}}} \sin\left(\frac{\Omega_{\mathrm{tot}}}{2} T\right) (\sigma_+ + \sigma_-) \right] |-z\rangle \right|^2 \tag{24}$$

$$= \frac{1}{1 + (\Delta/\Omega)^2} \sin^2\left(\frac{\sqrt{\Delta^2 + \Omega^2}}{2} T\right) . \tag{25}$$

This is a periodic sin-function with a Lorentian shaped amplitude which depends on the detuning Δ of the oscillating magnetic field relative to its field strength Ω.

We can learn two things from this: Firstly, the maximum probability to excite the two-level system depends only on the detuning Δ. It reaches its maximum for a resonant driving field ($\Delta = \omega - \omega_0 = 0$) and is basically zero for large detunings ($\Delta \gg \Omega$). Secondly, the system will oscillate between its ground state $|-z\rangle$ and $|+z\rangle$ in time. These oscillations are called *Rabi oscillations*. For zero detuning ($\Delta = 0$) the system will be in the excited state for $\Omega_{\mathrm{tot}} T = \Omega T = \pi$ (π-*pulse*) and will be in a superposition between ground and excited state when $\Omega T = \pi/2$ ($\pi/2$-*pulse*). This behaviour is shown in fig. 1.

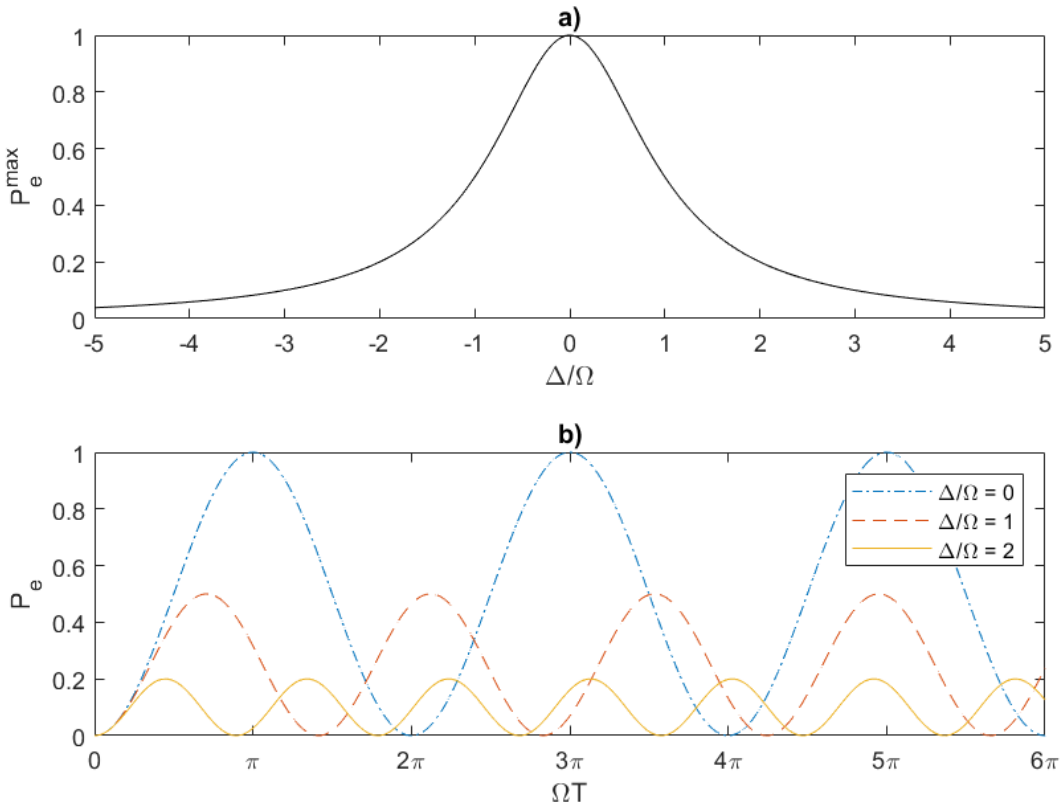

Figure 1: Excitation probability of a driven two-level system initially in the ground state. a) Maximum excitation probability $P_{\mathrm{e}}^{\max} = [1+(\Delta/\Omega)^2]^{-1}$ as a function of the relative detuning Δ/Ω. b) Excitation probability P_{e} as a function of pulse duration time T for different detunings Δ. The system performs *Rabi oscillations*.

3 Physical system

3.1 Diamond and color centers

Diamonds were first mentioned by Platon in Greece at around 4th century BC and were long used as gemstones for their shininess and rarity. Nowadays, its main application is industrial grinding and cutting where synthetically grown diamonds are used due their exceptional hardness.

Diamond can be created by *High Temperature High Pressure (HPHT)*, which mimics its natural growth conditions but adds molten metal as a solvent. To grow diamond of high purity, *Chemical Vapour Deposition (CVD)* is mostly used, where carbon is deposited from the gaseous phase (e.g. methane) onto a substrate. Diamond nano-crystals can be created by the explosion of a carbon source under oxygen deficiency (*detonation diamond*).

Its only constituents, carbon atoms, form a regular lattice, the *diamond lattice*. To achieve those very strong covalent bonds, the energy levels of carbon hybridize. While an isolated carbon atom has two electrons on the the 2s and 2p levels, they are hybridized to the sp3-level to form a tetrahedron with a binding angle of about 109.5° (see fig. 2). Pure diamond has a bandgap of 5.5 eV and is optically transparent. Some impurities form atomic-sized defects in the lattice which can emit visible light. These are called *color centers* and diamond can host a multitude of those. One famous example is the *Hope diamond*, which has boron impurities giving it its dark blue color. Recent studies show color centers are used for a variety of applications, such as in quantum nanophotonics, bio labelling, light emitting diodes, and spintronics. Some of these defects, namely the nitrogen vacancy (NV), the silicon vacancy (SiV) have been subject to rigorous research owing to their relatively known crystallographic and electronic structures.

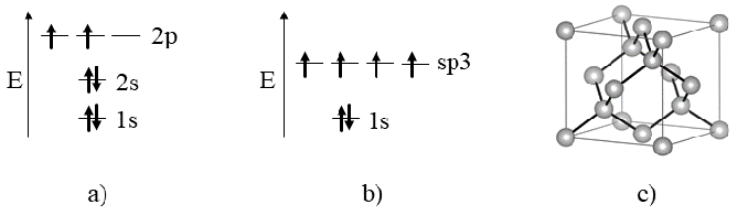

Figure 2: Hybridization of carbon and the diamond lattice. a) Energy levels of an isolated carbon atom. b) sp3-hybdridization of carbon which forms the diamond lattice. c) Atomic structure of the diamond lattice.

3.2 Nitrogen-vacancy center

3.2.1 Atomic structure and creation

The nitrogen-vacancy (NV) center is a color center in diamond, where one carbon atom is removed (vacant lattice site) and another neighbouring carbon atom is substituted with a nitrogen atom. It exists in two charge states, the negatively charged NV- and the neutral NV^0. Since most applications rely on the additional electron, we will use *NV center* synonymous for the negatively charged state.

As nitrogen is the most abundant impurity in diamond, the NV center was first discovered in the 1970s and has since been extensively studied. It shows spin-optical properties at room temperature which, together with diamond's exceptional stability, enables its use in a variety of applications without the need for additional cooling or vacuum.

The NV center's symmetry axis is placed along the one of the four diamond lattice orientations: [111], $[\bar{1}\bar{1}1]$, $[\bar{1}1\bar{1}]$, $[1\bar{1}\bar{1}]$. Its (electrical) dipole, responsible for fluorescence emission, is orthogonal to this axis. Therefore, the main emission of the NV center's farfield is also along its specific lattice orientation [10]. The NV center's lattice structure is shown in fig. 3.

To create a NV center, one has two general possibilities. Due to naturally occurring contamination of diamond with nitrogen, one can use this already present nitrogen and additionally create crystal damage (vacancies) by particle irradiation (e.g. ions, electrons). Another approach is to use an ultra-pure diamond sample and implant nitrogen into it, which creates vacancies at the same time. The diamond will be heated (*annealed*) to about 800 °C to help the nitrogen and vacancy diffuse together to form an NV center. Recently, it has been demonstrated that it is also possible to use highly energetic laser pulses on a nitrogen-rich sample to create NV centers. Firstly, the laser pulses create vacancies and, as a second step, it anneal the diamond locally until color centers are formed [2].

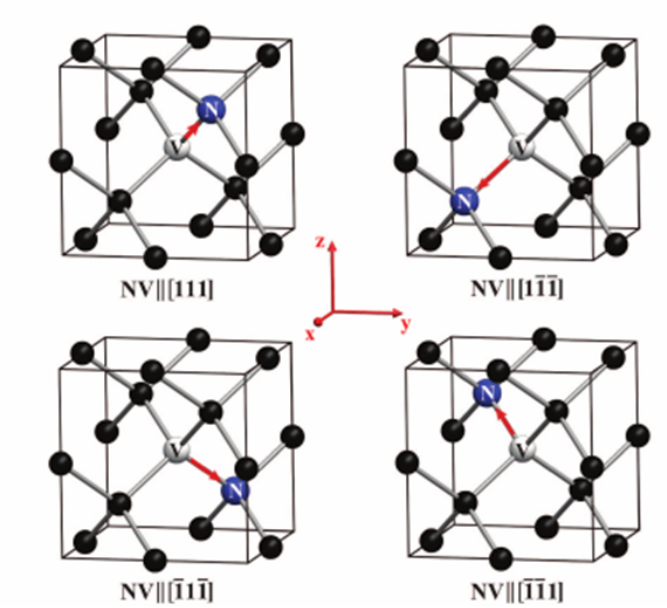

Figure 3: Atomic structure of the NV center. The arrow indicates its symmetry axis along one of the four diamond lattice orientations (111), ($\bar{1}\bar{1}$1), ($\bar{1}$1$\bar{1}$) and (1$\bar{1}\bar{1}$). Since the (electrical) dipole is orthogonal to the symmetry axis, the main farfield emission will be in the direction of the symmetry axis. Figure taken from [10].

3.2.2 Fluorescence spectrum

The NV center can be excited with an energy larger than the energy difference between its ground and excited state, 1.945 eV. This energy can be delivered by a laser with a wavelength $\lambda \leq 637\,\text{nm}$ according to *Planck's law*

$$E = h\nu = h\frac{c}{\lambda}\,, \tag{26}$$

where h is Planck's constant, ν the frequency and c the speed of light.

Using non-resonant excitation, the system is excited into a higher vibronic band of the excited state $|e\rangle$ and decays to the vibronic ground state of $|e\rangle$ within picoseconds. Emission into the zero-phonon line (ZPL) happens, when the system decays from the vibronic ground state of $|e\rangle$ into the vibronic ground state of its ground state $|g\rangle$ (lifetime of about 10 ns). Not only absorption but also emission can leave the system in a higher vibronic state. Consequently, the system can gain or loose energy by absorption or excitation of a vibronic state of the surrounding diamond lattice. Quantized excitation of a lattice are called *phonons*. The excitation of phonons is the dominating process for the NV center, which explains a relatively small emission into the ZPL at 637 nm but a prominent phonon sideband (PSB) shifted to longer wavelengths with a width of about 100 nm (see fig. 4).
The fluorescence spectrum can be explained with an energy diagram. This diagram will be discussed in the next section and will lead us directly to optically detected magnetic resonance (ODMR).

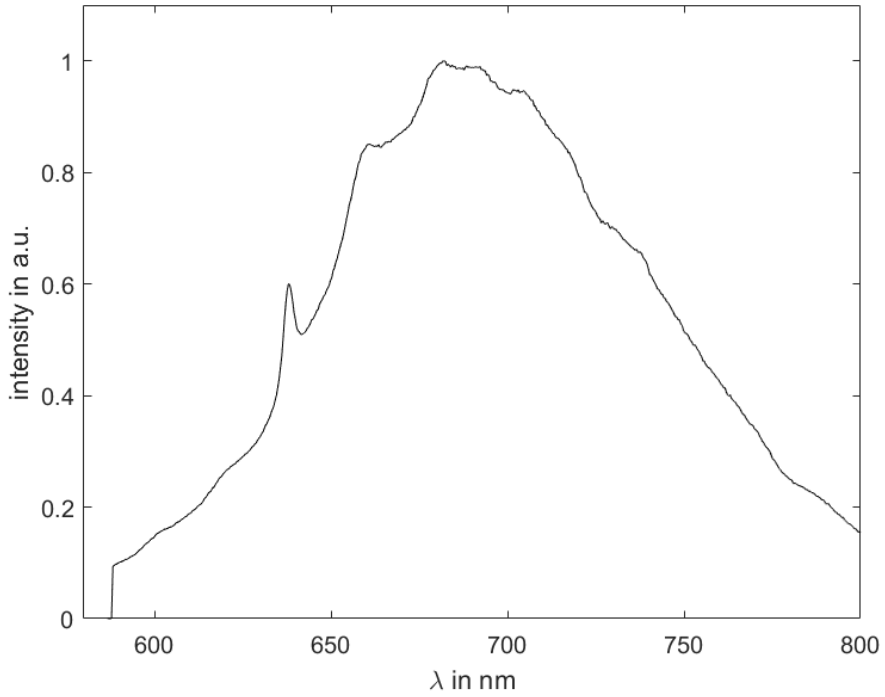

Figure 4: Fluorescence spectrum of the NV center at room temperature under excitation with a green (532 nm) laser. The spectrum shows small emission into the ZPL at 637 nm and the characteristic PSB at higher wavelengths with a width of approx. 100 nm.

3.3 Optically detected magnetic resonance (ODMR)

3.3.1 Energy diagram

The energy diagram of the NV center can be seen in fig. 5. This diagram visualizes the structure of the main energy levels and their spin-subsystems. In general, the NV center has three main energy levels, the ground state $|g\rangle$, the excited state $|e\rangle$ and a singlet state $|s\rangle$. Additionally, the ground and excited states are split into a spin-1 subsystem with magnetic spin numbers $m_s = 0, \pm 1$.

The $m_s = \pm 1$ states are nearly degenerate with no external magnetic field and are separated from the $m_s = 0$ state by the zero-field splitting $D_g = 2.87\,\mathrm{GHz}$. When an external magnetic field is applied, the $m_s = \pm 1$ states will split by an energy difference of $2\hbar\gamma B_{\parallel}$ according to the Zeeman effect.

Upon optical pumping, e.g. with a green (532 nm) laser, something remarkable happens: The $|g,0\rangle$ state will be excited to vibronics levels of $|e,0\rangle$ and mostly decay back to the $|g,0\rangle$ ground state under emission of a photon. The $|g,\pm 1\rangle$ state on the other hand will be excited to vibronic levels of $|e,\pm 1\rangle$ and predominantly decay non-radiatively through the singlet state $|s\rangle$ to the $|g,0\rangle$ ground state. There are two important consequences: Firstly, the $|\pm 1\rangle$-sublevel shows less fluorescence and, secondly, continuous optical pumping will polarize the system to the $|0\rangle$-sublevel. This is called *spin polarization*.

We conclude that we can initialize the spin-sublevel to the $|0\rangle$ state by extended laser excitation and read out the current spin-state by probing the fluorescence signal with a short laser pulse. High fluorescence indicates the $|0\rangle$ sub-state and low fluorescence indicates the $|\pm 1\rangle$ sub-state.

3.3.2 Manipulation of the spin-states and its application

The magic of the NV center relies on the combination of the optical readout of the spin state ($|0\rangle$ or $|\pm 1\rangle$) in combination with the a zero-field splitting D_g in the gigahertz-range.

This means, that the transition between this two-level system can be driven with an oscillating magnetic field with frequency ω. Since D_g is in the gigahertz-range, we will use a microwave (MW) source for this. The system will perform Rabi oscillations with Rabi frequency $\Omega \propto B_{\perp}$, which depend on the amplitude of the applied MW field. We call a plot of the fluorescence intensity I over the applied MW frequency ω the ODMR (*optically detected magnetic resonance*) spectrum. There are different methods to aquire this spectrum. We will focus on *cw*-ODMR, in which the laser and MW are continuously applied and the MW frequency is swept. There are pulsed measurement schemes, which can be understood by applying the Rabi model, but those require more complex equip-

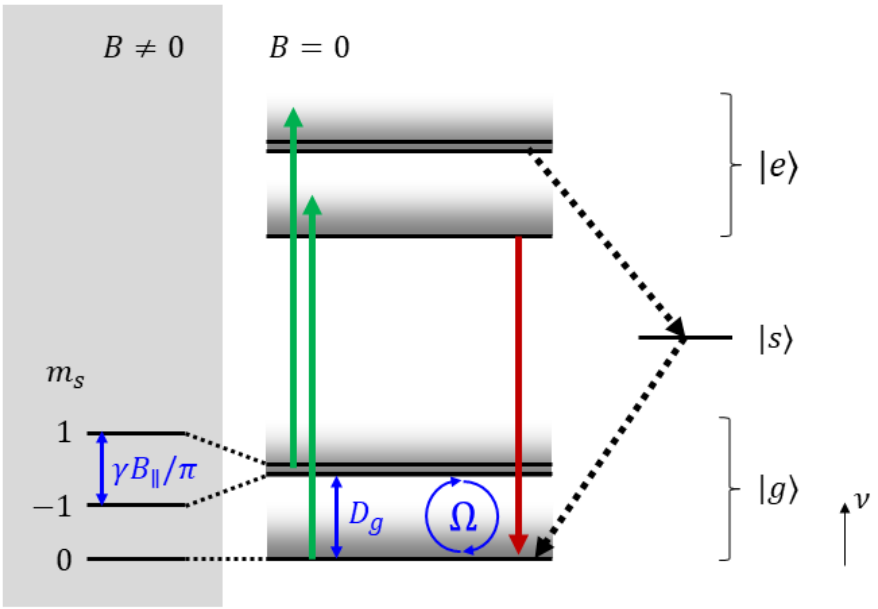

Figure 5: Simplified energy diagram of the NV center. The frequency axis (ν) is not to scale. Radiative transitions are marked as solid while non-radiative decays are marked as dotted arrows. There exists a ground state $|g\rangle$, an excited state $|e\rangle$ and a singlet state $|s\rangle$. Their additional vibronic states are shaded in grey. Ground and excited state feature a spin-1 sublevel with magnetic spin numbers $m_s = 0, \pm 1$. Those are split by the zero-field splitting $D_g = 2.87\,\mathrm{GHz}$. The transition between them can be driven with Rabi frequency Ω. Upon application of an external magnetic field, the $m_s = \pm 1$ sublevel split by $\gamma B_\parallel / \pi$, where $\gamma/2\pi \approx 28.025\,\mathrm{MHz\,mT^{-1}}$. $|e,0\rangle$ will radiatively decay to $|g,0\rangle$. $|e,\pm 1\rangle$ will predominantly decay non-radiatively through $|s\rangle$ to $|g,0\rangle$.

ment and are not part of this lab course.

The ODMR spectrum will not only allow the calculation of D_g but, since the magnetic sub-levels are split by $\gamma B_\parallel/\pi$, also the strength of a static external magnetic field $B_\parallel$. In principle, one resonance for each crystallographic axis will be visible. Depending on the diamond orientation relative to the magnetic field, e.g., parallel to the [111]-direction, some of them might merge to an indistinguishable resonance dip with a higher contrast (see fig. 6). In general, the contrast of the resonances depends on the orientation of the electrical and magnetic dipole in regards to the experimental setup. The laser polarization defines the electric field at the focus. The collection efficiency depends on the electrical dipole orientation and the NA of the objective. The transition frequency of the spin-subsystem depends on the MW polarization.

It has been shown that the splitting between the m_s sub-levels also depends on temperature, external electric fields and lattice strain which further enables the NV center's use as a single atom sensor. These effects, however, are not easily distinguishable which complicates the application as a multi-parameter sensor. Nonetheless, possible applications of the NV center and ODMR in particular range from quantum cryptography [1] and quantum memory [6] to magnetic [3] and electric [5] field and temperature sensing [13] to the violation of Bell-inequalities [8].

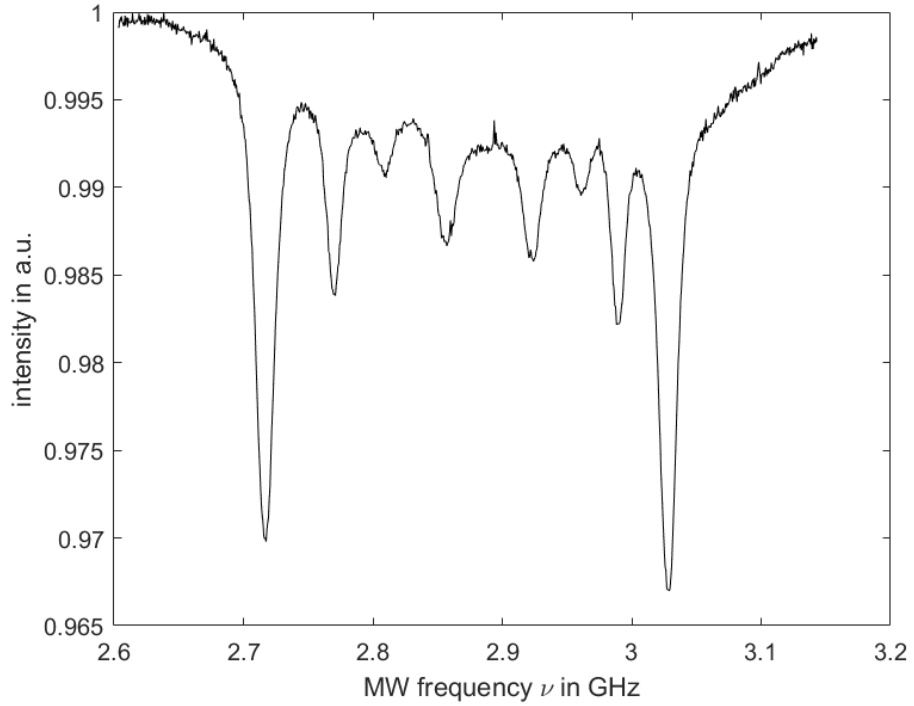

Figure 6: ODMR spectrum of an NV center ensemble with an external magnetic field aligned at 45° to the [111] crystal axis. Eight-fold splitting of the resonances is visible.

4 Experimental setup and procedure

4.1 Setup

As discussed in the theory, measuring ODMR requires three main ingredients: Firstly, we need a strong light field (e.g. a laser) to excite the NV centers. Secondly, we need to collect the fluorescence signal and, thirdly, we need to apply a magnetic field with microwave frequency to drive the spin-sublevels.

In this experiment, we excite the NV centers using a 5 mW, 532 nm diode laser (*Thorlabs CPS532*) in a home-built confocal microscopy setup. The laser intensity is controlled using a variable neutral density filter. The sample is excited through a 50x 0.95 NA objective (*Zeiss C Epiplan-Apochromat 50x/0.95 DIC M27*) which is mounted on a transnational z-stage for efficient excitation and fluorescence signal collection. The sample, single-crystalline NV rich diamond sample (2.6 mm x 2.6 mm x 1 mm), is placed on a planar antenna which provides a strong, homogeneous, broadband magnetic field [11] (see fig. 7b). The antenna along with the sample is placed on x-y-stage to align their position relative to the microscope objective.

To generate the microwave signal, which drives the Rabi oscillations, we use a voltage-controlled oscillator (VCO, *Mini-Circuits TB-ROS-3050C+*). The VCO's input voltage is fed by a Labview-controlled function generator (*Keysight 33210A*), whose output signal is amplified by an operational amplifier circuit (amplification $A = 1.5$) to match the VCO's input range of 1.5 V to 15 V. The microwave signal is amplified by an amplifier (*Mini-Circuits ZRL-3500+*) to a power of more than 20 dBm at a spectral bandwidth of 0.1 MHz (see fig. 7a). The signal is transmitted to the antenna by SMA cables. The calibration data of this circuit (tuning voltage vs. microwave frequency) can be found in the appendix.

The static magnetic field is created with a solenoid and a current source. You can assume the following parameters for the solenoid: Number of windings $N = 302$, average radius $R = 28.9$ mm and length $l = 18$ mm. These values have errors smaller than 5 %. The current will be varied from 0 A to 1.6 A. The solenoid axis is angled at about 30° with respect to the z-axis.

From the objective the signal is sent through a 550 nm dichroic mirror (*Semrock Di03-R532*) which transmits light that has a wavelength larger than 550 nm (fluorescence) and reflects light below that wavelength (laser). To ensure that no residual laser light goes to the detectors, an additional 550 nm longpass filter (*Thorlabs FELH0550*) is placed along the detection path, which reflects all light with wavelengths below 550 nm. Before the detection, a pinhole (50 µm diameter) can be placed at the common focus point of

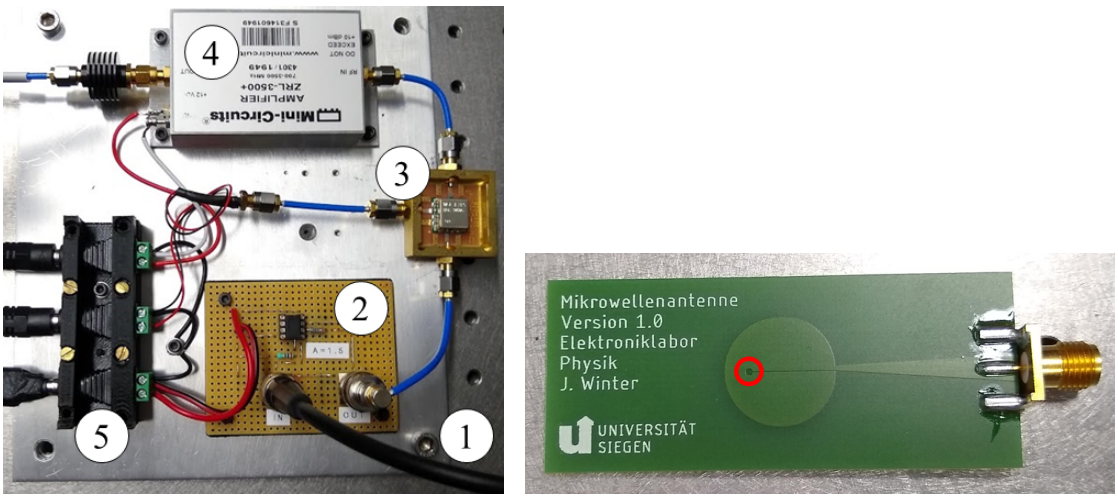

(a) (b)

Figure 7: (a) Microwave circuit. 1. Tuning voltage input. 2. Operational amplifier (amplification $A = 1.5$). 3. Voltage-controlled oscillator (VCO). 4. Microwave amplifier. 5. DC power supplies. (b) Planar microwave antenna with SMA connector. The red circle indicates the proper diamond sample position.

two lenses (confocal), which can be placed in the beam path and limits the collection volume to the confocal volume. This helps to suppress unwanted background (such as a sample holder). By assuming a focused Gaussian beam, one can show that the confocal dimensions (Airy disc Δr and depth of field Δz) are

$$\Delta r \approx 0.61 M \frac{\lambda}{\mathrm{NA}} \quad \text{and} \quad \Delta z \approx 2M^2 \frac{\lambda}{\mathrm{NA}^2} \,, \tag{27}$$

where M is the magnification of the objective, NA is its numerical aperture and λ the wavelength of the fluorescence signal [9].

There are different types of detectors that are used in the setup. By flipping a mirror in the beam path, the light gets reflected to the corresponding detector. We use a CMOS (complementary metal–oxide–semiconductor) camera (*Thorlabs DCC1645C*) to align the laser beam and to check the alignment of the confocal setup. In addition, it helps to image the fluorescence signal using proper filters. A spectrometer (*Oceanoptics QEPro*) is used to characterize the fluorescence signal and to make sure that NV centers are excited. By integrating over the NV spectrum and varying the applied MW frequency, we can use the spectrometer to measure ODMR.

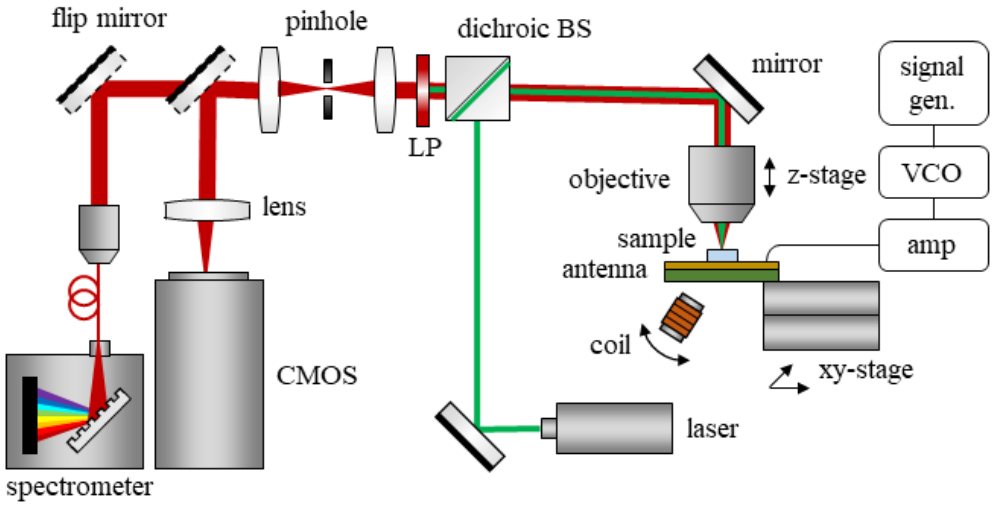

(a)

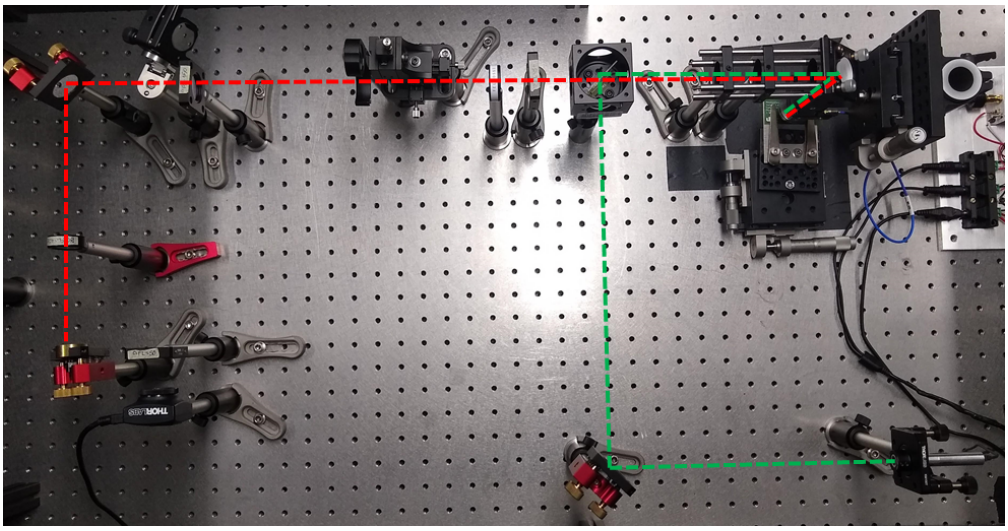

(b)

Figure 8: (a) Experimental setup sketch. (BS) Beamsplitter. (CMOS) Complementary metal–oxide–semiconductor. (LP) Longpass filter. (VCO) Voltage-controlled oscillator. (b) Image of the real setup. Red and green lines are added to indicate the laser and fluorescence beam path.

4.2 Experimental tasks

1. Wear laser safety goggles.

2. Now, turn on the laser and wait for five to ten minutes until it stabilizes its output power.

3. Open the Oceanview software, select *Quickview* and change the integration time to 10 ms.

4. Focus the laser beam on the diamond surface by turning the micrometer screw on the z-stage. Find an area on the sample, where you can see a clear NV ZPL on the spectrum. You can move the diamond sample relative to the objective by turning the micrometer screws on the x- and y-stage. Make sure to limit unwanted signal from the substrate. Wait for a stable ZPL and a good signal-to-noise-ratio. When you found a satisfying signal, take a spectrum and save it to a .txt-file.

5. Close the Oceanview software, open the Labview ODMR software. In the ODMR software, set the exposure time to a suitable value (e.g., 20 ms), select a voltage from 1 V to 10 V with a step size of 10 mV steps. The spectrum is automatically integrated from 600 nm to 800 nm to create the ODMR signal. The data is saved into the sub-folder *data* within the *ODMR* folder. The voltage is saved in the first column and the intensity is saved in the second column of the file. The columns are separated by semi-colons. Select refresh in the drop-down menu and afterwards connect to the signal generator by selecting it in the drop-down menu. Press *connect devices*. You should hear a click from the relais inside the signal generator. Now, click *start measurement*. If you want to repeat the measurement, click on the arrow in the top left corner, click *connect devices* and then, again, *start measurement*. You can use this first measurement to characterize the laser fluctuations.

   A screenshot of this Labview program is shown in fig. 9.

6. You can now connect the MW antenna.

7. Unplug the cables from the solenoid. Switch on the lab power supply to check that it is set to its minimum current value. You can switch between current control and voltage control by turning the corresponding knob. Now, connect the solenoid to the power supply. Remember, that you may not exceed the solenoid's maximum current rating of 1.6 A. Place the solenoid as close to the antenna as possible. Measure/estimate the distance between the sample and the solenoid's center. You can read the exact current from the multi-meter, which is connected in line with the solenoid and the power supply.

8. Select a high current (max. $I = 1.6\,\mathrm{A}$) to generate a strong external magnetic field such that eight distinct resonances are visible, when you measure the ODMR

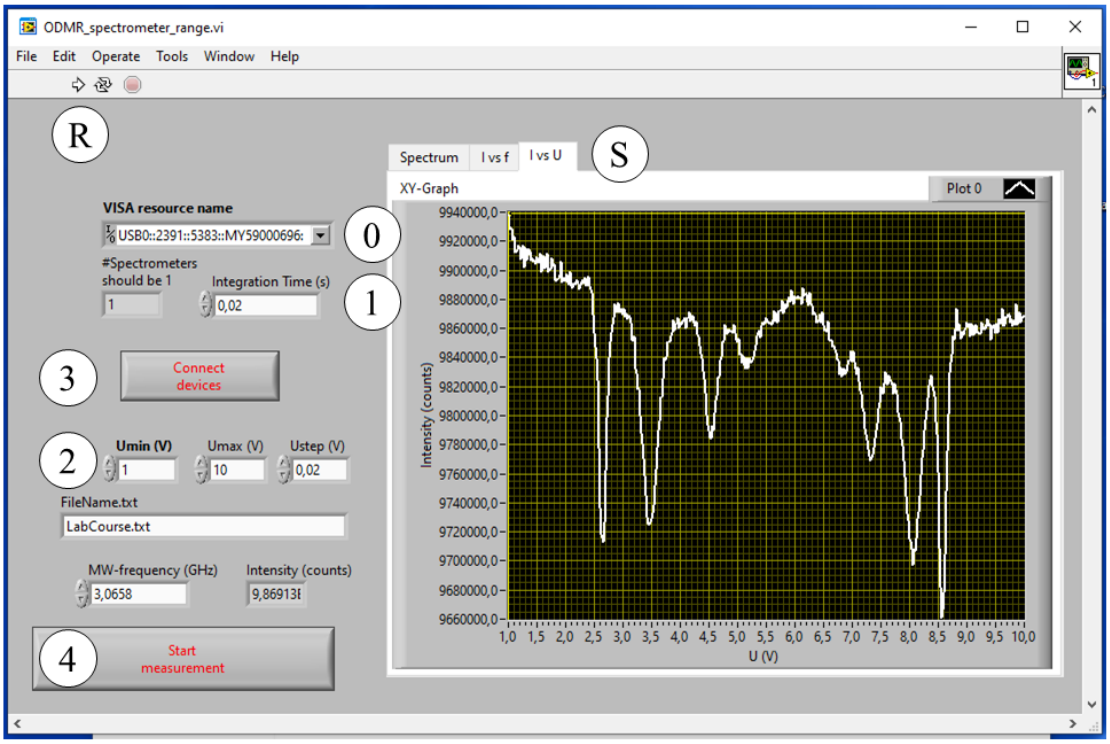

Figure 9: Screenshot of Labview prorgam. The operational steps are the following: 0. Use the dropdown menu. Click refresh. Select the function generator. 1. Specify the integration time of the spectrometer. A time of $0.01 - 0.02\,\mathrm{s}$ should be sufficient. 2. Define the tuning voltage interval ($U = 1 - 10\,\mathrm{V}$) and the step size. For a fast sweep, you can use $\Delta U = 50\,\mathrm{mV}$. It is recommended to not go below $\Delta U = 5\,\mathrm{mV}$ because of a rising acquisition time. Usually. $\Delta U = 10\,\mathrm{mV}$ is a good trade-off between acquisition time and resolution. 3. Connect the devices. You should hear a click from the relais inside the signal generator. 4. Start the measurement. R. If you want to start a new measurement, click on the arrow and repeat steps $1-4$. S. You can observe the fluorescence spectrum, and the ODMR spectrum (I vs. ν and I vs. U) by changing the index tab.

spectrum. If that is not the case, rotate the diamond sample and or vary the current until they are visible. Take a picture of the position of the diamond sample on the sample holder relative to the solenoid once it is well aligned.

9. Sweep the solenoid current from 0 A to 1.6 A in 200 mA steps. Measure the ODMR spectrum each time (1 V to 10 V with step size of 10 mV).

10. Lastly, check that all your data is saved properly. You need a picture of the alignment of the sample relative to the solenoid. Additionally, you need an ODMR spectrum with a disconnected antenna and eleven ODMR spectra with a connected antenna and a varied external magnetic field ($I = 0 - 1.6\,\mathrm{A}$).

4.3 Analysis tasks

1. Plot the fluorescence spectra (NV and its background) in one figure.

2. The calibration data for the microwave circuit (tuning voltage $U \leftrightarrow$ microwave frequency ν) can be found in the appendix. You can either use linear interpolation or a first to third order polynomial to do a fit. Explain why you chose your method (ease of use, uniform residuals...). Use this calibration for all further data analysis.

3. Plot the fluorescence fluctuations, which (mostly) correspond to the laser fluctuations, measured without MW antenna over time. You get the time scale from the integration time and the voltage steps. Characterize the fluctuations by their signal to noise ratio SNR = amplitude/standard deviation.

4. Plot all measured ODMR spectra with axes intensity, ν and solenoid current I. Sort them in terms of I. Suitable plot types for such three-dimensional datasets are, e.g., *pcolor* in matplotlib or Matlab, *waterfall* in Matlab.

5. Determine the zero-field splitting $D \pm E$ (for $I = 0\,\mathrm{A}$) and its error by fitting two Lorentzians plus linear background $f(\nu)$

$$f(\nu) = \frac{A_1}{1 + [(\nu - D - E)/\Gamma_1]^2} + \frac{A_2}{1 + [(\nu - D + E)/\Gamma_2]^2} + C\nu + F \tag{28}$$

   to the zero-field ODMR spectrum. A_i are the amplitudes and Γ_i their full width at half maximum (FWHM). C and F are the fit parameters of the linear background. It will be helpful to provide starting values and upper and lower bounds to the fit parameters. Specify the error of D and E. Plot the data set and your fit function together in one figure.

6. Fit the ODMR spectrum with the largest external magnetic field with Lorentzian functions. Eight dips should be visible. Instead of fitting the sum of eight Lorentzians, it might be sufficient to fit each dip separately with a single Lorentzian and a linear background of the form $g_i(\nu)$

$$g_i(\nu) = \frac{G_i}{1 + [(\nu - \nu_{0,i})/\Gamma_i]^2} + H_i\nu + K_i \ , \tag{29}$$

   where G_i is the amplitude of the dip, $\nu_{0,i}$ the position of its center, Γ_i its FWHM and $i \in [1; 8]$. H_i and K_i are the fit parameters of the linear background. Specify ν_0 and Γ and their errors. It is highly recommended to provide starting values and upper and lower bounds to the fit parameters. Plot the data set and the fitted functions in their range together in one figure.

7. You can assume a symmetric splitting of all dips around D due to their magnetic spin number $m_s = \pm 1$. Their energy (frequency) difference is

$$h\,\Delta\nu_0 = \Delta E = 2\,\hbar\gamma B_i\ , \tag{30}$$

where B_i is the magnetic field parallel to their crystal axis and $\gamma/2\pi \approx 28.025\,\mathrm{MHz\,mT^{-1}}$. Therefore, you can determine the parallel external magnetic field B_i and its error for each of the four crystal axes.

8. We will now determine the magnitude[1] of the external magnetic field.

   - Assume the crystal axes are

$$\boldsymbol{e}_1 = \boldsymbol{e}_z\ , \tag{31}$$
$$\boldsymbol{e}_2 = \sin(\alpha)\cos(\beta)\boldsymbol{e}_x + \sin(\alpha)\sin(\beta)\boldsymbol{e}_y + \cos(\alpha)\boldsymbol{e}_z\ , \tag{32}$$
$$\boldsymbol{e}_3 = \sin(\alpha)\cos(\beta)\boldsymbol{e}_x - \sin(\alpha)\sin(\beta)\boldsymbol{e}_y + \cos(\alpha)\boldsymbol{e}_z\ , \tag{33}$$
$$\boldsymbol{e}_4 = \sin(\alpha)\boldsymbol{e}_x + \cos(\alpha)\boldsymbol{e}_z\ , \tag{34}$$

     where $\alpha = 109.5°$ and $\beta = 120°$.

   - Calculate the unit vectors in x-, y-, and z-direction in terms of crystal axis vectors. Calculate B_x, B_y and B_z in terms of the B_i accordingly. For example, the unit vector of the x-axis can be calculated by

$$\boldsymbol{e}_x = [\boldsymbol{e}_4 - \cos(\alpha)\boldsymbol{e}_1]/\sin(\alpha) \tag{35}$$

     and, consequently, the magnetic field in x-direction B_x is

$$B_x = [B_4 - \cos(\alpha)B_1]/\sin(\alpha)\ . \tag{36}$$

   - You can determine the absolute value $|B|$ by

$$|B| = \sqrt{B_x^2 + B_y^2 + B_z^2}\ . \tag{37}$$

[1] One can actually also determine the orientation of the magnetic field using NV centers. To do so, one has to know the crystal orientation corresponding to the ODMR resonances. This can be done with an static external magnetic field aligned along one of the crystal axes [12] or with polarimetry.

- You now know the amplitude of the external magnetic field $\boldsymbol{B}$. Compare this to the analytical solution of the on-axis magnetic field of a solenoid B_s

$$B_s(\rho = 0, z) = \frac{\mu_0 I N}{2} \left(\frac{l/2 - z}{l\sqrt{R^2 + (l/2 - z)^2}} + \frac{l/2 + z}{l\sqrt{R^2 + (l/2 + z)^2}} \right) , \quad (38)$$

  where N is the number of turns, I is the solenoid current, l is the length of the solenoid and R its radius. ρ is the radial and z is the axial distance from the center (!) of the solenoid. The solenoid axis is angled at about 30° with respect to the z-axis. Estimate the errors for ρ and z from the setup. Accompany this with the picture you took from the sample and the solenoid. Compare this analytical solution to the B-field determined by ODMR.

9. Compare your results of the external magnetic field $|B|$ with the ODMR spectra plotted in the diagram. Give an estimate of the minimum external magnetic field needed to resolve all eight resonances. The parameter Γ from the Lorentzian fits might be useful for this.

10. To summarize, we would like you to: Plot the three fluorescence spectra. Calibrate the microwave circuit and plot the ODMR spectra for multiple solenoid currents. Determine the zero-field splitting. At a large external magnetic field, determine the B-field amplitude and compare it to the analytical model of the solenoid used to generate the field.

4.4 Output requirements

A good lab report does more than presenting data; it demonstrates the writer's comprehension of the concepts behind the data. Merely recording the expected and observed results is not sufficient; you should also identify how and why differences occurred, explain how they affected your experiment, and show your understanding of the principles the experiment was designed to examine. Bear in mind that a format, however helpful, cannot replace clear thinking and organized writing. You still need to organize your ideas carefully and express them coherently.

Typical components to be fulfilled are: Title Page, Abstract, Introduction, Methods and Materials (or Equipment), Experimental Procedure, Results, Discussion, Conclusion, References. Figures should have figure captions with explanations. All graphs should have labeled axes and visible data points and curves. Curve fits and fitted parameters should be included. All quantities should be followed by the calculated error.

If at any point during your data processing or report writing you have any doubts, you are encouraged to contact your teaching assistants. We are more than happy to help you finish your task and learn as much as possible. We wish you good luck with your experiments!

Appendix

Table 1: Calibration data for microwave source (tuning voltage U vs. microwave frequency ν and power P.)

U (V)	ν (GHz)	P (dBm)
1.0	2.602	20.0
1.2	2.606	
1.4	2.610	
1.6	2.626	
1.8	2.640	
2.0	2.652	22.0
2.2	2.664	
2.4	2.674	
2.6	2.684	
2.8	2.696	
3.0	2.706	22.1
3.2	2.718	
3.4	2.730	
3.6	2.740	
3.8	2.752	
4.0	2.764	22.2
4.2	2.776	
4.4	2.788	
4.6	2.796	
4.8	2.814	
5.0	2.828	22.2
5.2	2.842	
5.4	2.854	
5.6	2.870	
5.8	2.882	
6.0	2.896	22.2
6.2	2.910	
6.4	2.926	
6.6	2.932	
6.8	2.954	
7.0	2.968	22.2
7.2	2.982	
7.4	2.996	
7.6	3.010	

continued on next page

Table 1: Calibration data for microwave source (continued).

U (V)	ν (GHz)	P (dBm)
7.8	3.024	
8.0	3.036	22.4
8.2	3.056	
8.4	3.062	
8.6	3.074	
8.8	3.084	
9.0	3.094	22.5
9.2	3.104	
9.4	3.114	
9.6	3.122	
9.8	3.130	
10.0	3.136	21.8

References

[1] Alexios Beveratos et al. „Single Photon Quantum Cryptography.“ In: *PRL* 89.18 (Oct. 2002), p. 187901. URL: https://link.aps.org/doi/10.1103/PhysRevLett.89.187901.

[2] Yu Chen Chen et al. „Laser writing of individual nitrogen-vacancy defects in diamond with near-unity yield.“ In: *Optica* 6.5 (2019), p. 662. DOI: 10.1364/optica.6.000662.

[3] C. L. Degen. „Scanning magnetic field microscope with a diamond single-spin sensor.“ In: *Appl. Phys. Lett.* 92.24 (June 2008), p. 243111. ISSN: 0003-6951. DOI: 10.1063/1.2943282. URL: https://doi.org/10.1063/1.2943282.

[4] Wolfgang Demtröder. *Experimentalphysik 3*. Jan. 2016. ISBN: 978-3-662-49093-8. DOI: 10.1007/978-3-662-49094-5.

[5] F. Dolde et al. „Electric-field sensing using single diamond spins.“ In: *Nature Physics* 7.6 (2011), pp. 459–463. ISSN: 1745-2481. URL: https://doi.org/10.1038/nphys1969.

[6] Torsten Gaebel et al. „Room-temperature coherent coupling of single spins in diamond.“ In: *Nature Physics* 2.6 (2006), pp. 408–413. ISSN: 1745-2481. URL: https://doi.org/10.1038/nphys318.

[7] Christopher Gerry and Peter Knight. *Introductory Quantum Optics*. Cambridge University Press, 2004. DOI: 10.1017/CBO9780511791239.

[8] B. Hensen et al. „Loophole-free Bell inequality violation using electron spins separated by 1.3 kilometres.“ In: *Nature* 526.7575 (2015), pp. 682–686. ISSN: 14764687. DOI: 10.1038/nature15759.

[9] Lukas Novotny and Bert Hecht. *Principles of Nano-Optics*. Cambridge University Press, 2006. DOI: 10.1017/CBO9780511813535.

[10] Linh Pham et al. „Enhanced metrology using preferential orientation of nitrogen-vacancy centers in diamond.“ In: *Physical Review B* 86 (July 2012). DOI: 10.1103/PhysRevB.86.121202.

[11] Kento Sasaki et al. „Broadband, large-area microwave antenna for optically detected magnetic resonance of nitrogen-vacancy centers in diamond.“ In: *Review of Scientific Instruments* 87.5 (2016), p. 053904. DOI: 10.1063/1.4952418. eprint: https://doi.org/10.1063/1.4952418. URL: https://doi.org/10.1063/1.4952418.

[12] S Steinert et al. „High Sensitivity Magnetic Imaging Using an Array of Spins in Diamond.“ en. In: *Rev. Sci. Instrum.* (), p. 6.

[13] David M. Toyli et al. „Fluorescence thermometry enhanced by the quantum coherence of single spins in diamond.“ In: *Proc Natl Acad Sci USA* 110.21 (May 2013), p. 8417. URL: http://www.pnas.org/content/110/21/8417.abstract.

[14] Haimei Zhang et al. „Little bits of diamond: Optically detected magnetic resonance of nitrogen-vacancy centers.“ In: *American Journal of Physics* 86.3 (2018), pp. 225–236. DOI: 10.1119/1.5023389. eprint: https://doi.org/10.1119/1.5023389. URL: https://doi.org/10.1119/1.5023389.